Supporting Information

Interface engineering of $Ni_9S_8/MoS_2/Ni_3S_2$ heterostructure to boost biomass upgrade coupled with hydrogen evolution reaction at large current densities

Ao Wang, Yan Meng, Gang Xu, Shi-Jiao Dong and Jun-Ling Song*

International Joint Research Center for Photoresponsive Molecules and Materials, School of Chemical and Material Engineering, Jiangnan University, Lihu Street 1800, Wuxi 214122, China

Experimental section

Reagents and materials: All reagents used in this study were purchased and directly used without further purification: $Ni(NO_3)_2·6H_2O$(AR), $Na_2MoO_4·6H_2O$(AR), and CH_4N_2S(AR) were purchased from Shanghai Titan Scientific Co., Ltd.. Nickel foam (NF) was purchased from Suzhou Cheng Er Nuo Technology Co. Ltd..

Physical characterizations: The structure of Ni-Mo-S is determined by PXRD (Bruker D8, Cu-Kα). the spectra were recorded in the 2θ range of 5° to 60°. The morphology of Ni-Mo-S were investigated by scanning electron microscopy (SEM, Hitach S-4800) and transmission electron microscope (TEM, JEOL 2100F). X-ray electron spectroscopy (XPS) was performed on AXIS Supra by Kratos Analytical Inc. Using monochromatized Al Ka radiation as X-ray source. All spectra were calibrated by C 1s (284.8 eV).

Product analysis:

The concentrations of HMF and oxidation products were determined by high

performance liquid chromatography (HPLC) system (Waters 1525) using a 4.6 × 250 mm NuovaSil C18-WH, 5μm column with detection wavelength set at 265 nm and column temperature maintained at 30 °C. The HPLC eluent was a mixture of solvent A (5 mM ammonium formate solution) and B (methanol). For the HMF oxidation reaction, isocratic elution separation was performed using 30% A and 70% B at a flow rate of 0.6 mL min^{-1} over 15 min. HPLC samples were prepared by diluting 1.0 mL of the reaction mixture with 49.0 mL of deionized water. Quantification of HMF and oxidation products was calculated from the calibration curve. The HMF conversion, the product yield, and the FE value of FDCA were calculated using the following equations, where F is Faraday's constant.

The conversion of HMF can be calculated by the following eqn:

$$Conversion = \frac{\text{n(reacted HMF)}}{\text{n(initial HMF)}} \times 100\%$$

The selectivity and yield of the FDCA were determined by the following eqn respectively:

$$Selectivity = \frac{n(FDCA\ production)}{n(reacted\ HMF)} \times 100\%$$

$$Yield = \frac{\text{n(FDCA production)}}{\text{n(initial HMF)}} \times 100\%$$

The faradaic efficiency of the product was calculated using eqn:

$$FE\ of\ FDCA = \frac{mol\ of\ FDCA\ formed}{total\ charge\ passed/(6 \times F)} \times 100\%$$

Electrochemical measurements: All electrochemical tests were carried out in a three-electrode system using a CHI760E electrochemical workstation (Shanghai Chenhua, China) without iR correction. HMFOR and OER were carried out in a typical three-electrode system with a H-type cell separated by an anion exchange membrane (N117

DuPont). Pt wire and Hg/HgO were used as counter electrode and reference electrode, the as-prepared Ni-Mo-S (1cm ×1cm) material was used as the working electrode. The measured voltage value is converted into the electrode potential *vs* the reversible hydrogen electrode (RHE) by the equation $E_{RHE}=E_{Hg/HgO}$ + 0.059×pH + 0.098 V. The electrochemical OER and HMFOR experiments were conducted in 50 mL of 1.0 M NaOH solution with and without 20mM HMF. Electrochemical impedance spectroscopy (EIS) measurements were recorded in the frequency range of 10^5– 0.1 Hz with an amplitude of 5 mV. The electric double layer capacitance of the prepared catalyst was determined by the CV of different scanning speeds (20, 40, 60, 80 and 100 mV s^{-1}). Without any iR correction.

$$NH_2CSNH_2 + 3H_2O \longrightarrow 2NH_4^+ + HS^- + HCO_3^-$$

$$3Ni + 2HS^- + 2H_2O \longrightarrow Ni_3S_2 + 2H_2 + 2OH^-$$

$$4NiMoO_4 + 9HS^- + 3H_2O \longrightarrow 4MoS_2 + SO_4^{2-} + 4Ni^{2+} + 15OH^-$$

$$9Ni^{2+} + 8HS^- + H_2 + 10OH^- \longrightarrow Ni_9S_8 + 10H_2O$$

Scheme. S1 Synthetic reaction equation

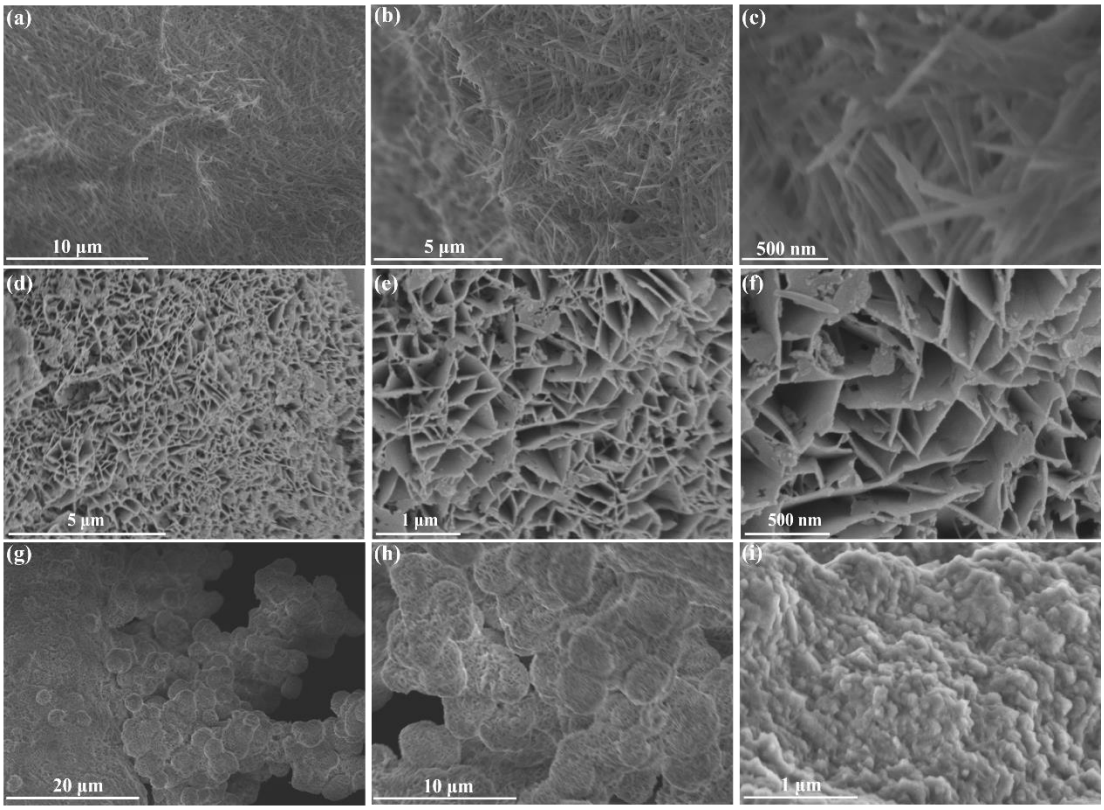

Fig. S1 (a-c) SEM images of Ni-Mo-O-1, (d-f) Ni-Mo-O-2 and (g-i) Ni-Mo-O-3

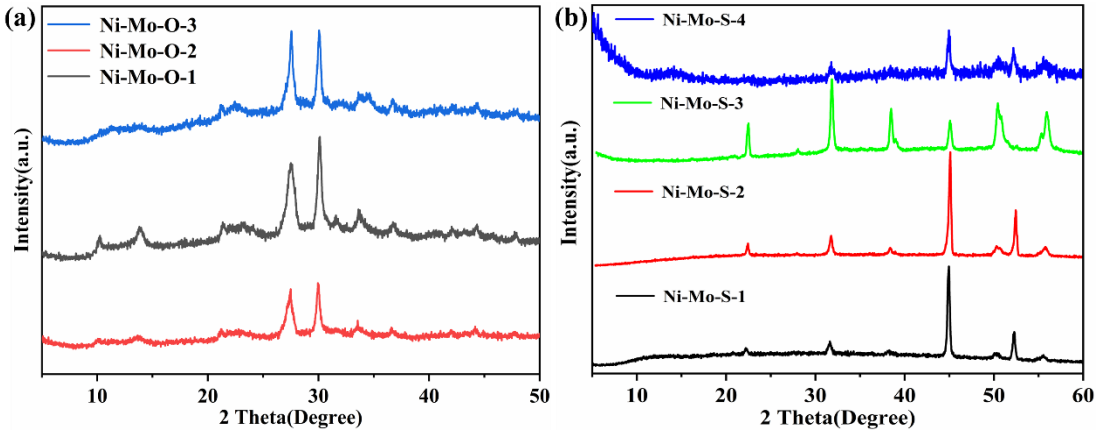

Fig. S2 XRD of powder scraped from (a) Ni-Mo-O-1, Ni-Mo-O-2 and Ni-Mo-O-3, (b) Ni-Mo-S-1, Ni-Mo-S-2, Ni-Mo-S-3 and Ni-Mo-S-4.

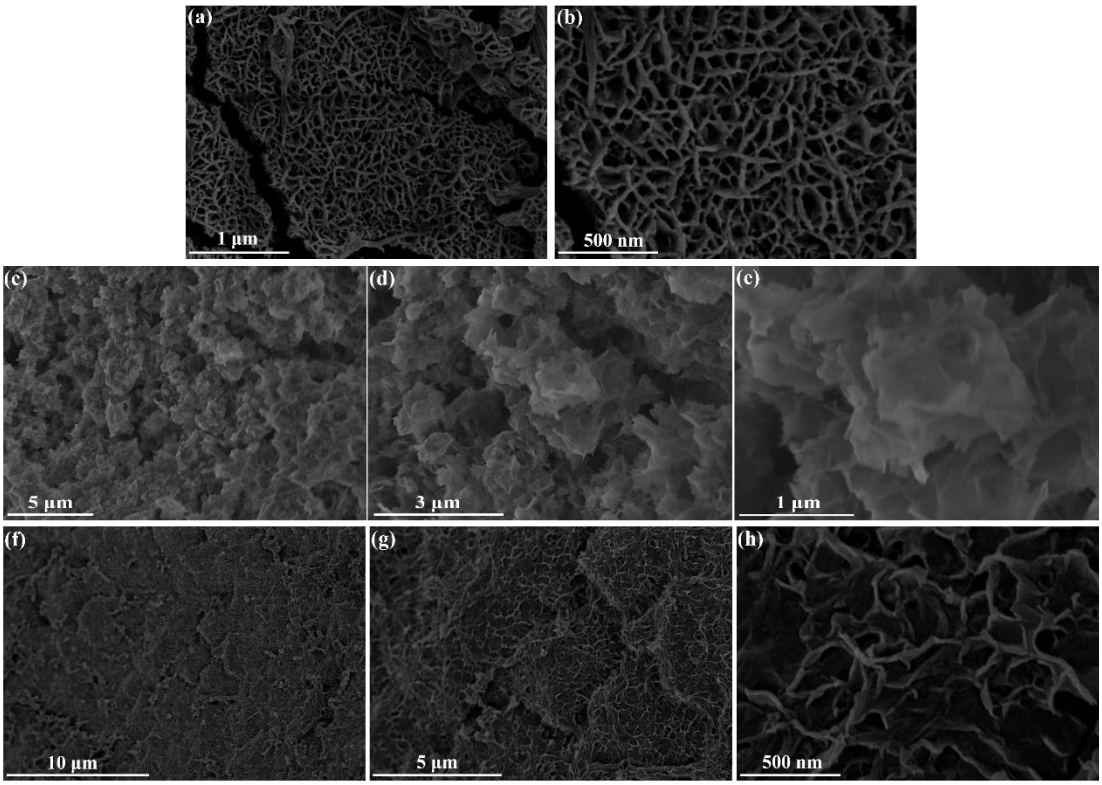

Fig. S3 (a-b) SEM images of Ni-Mo-S-1, (c-e) Ni-Mo-S-2 and (f-h) Ni-Mo-S-4

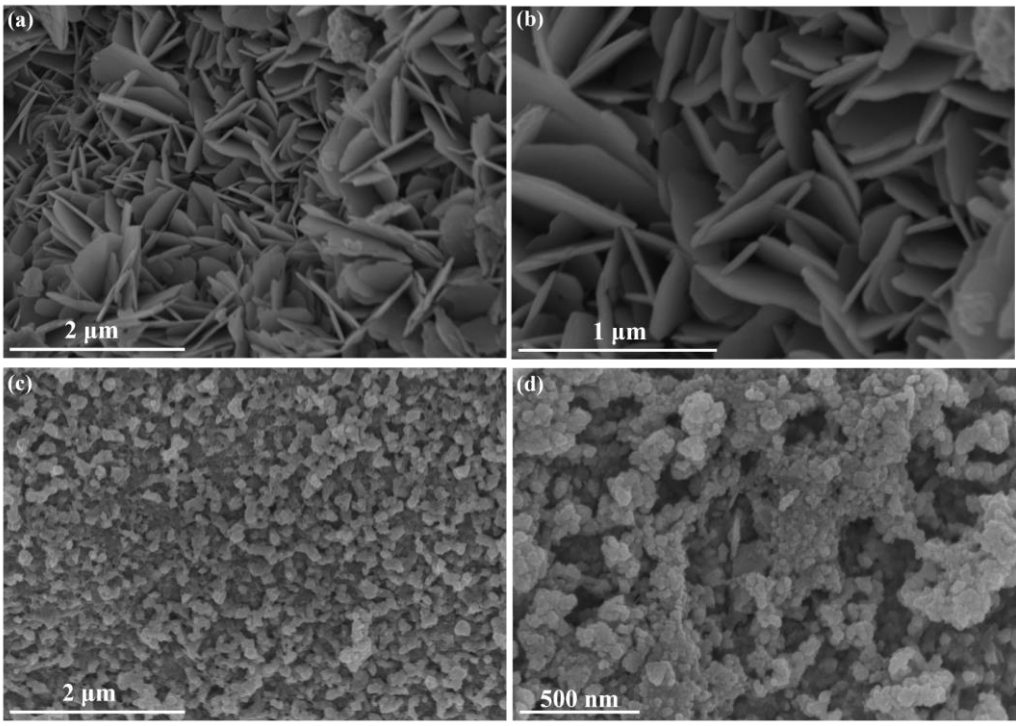

Fig. S4 (a-b) SEM images of Ni_3S_2/NF and (c-d) MoS_2/CC

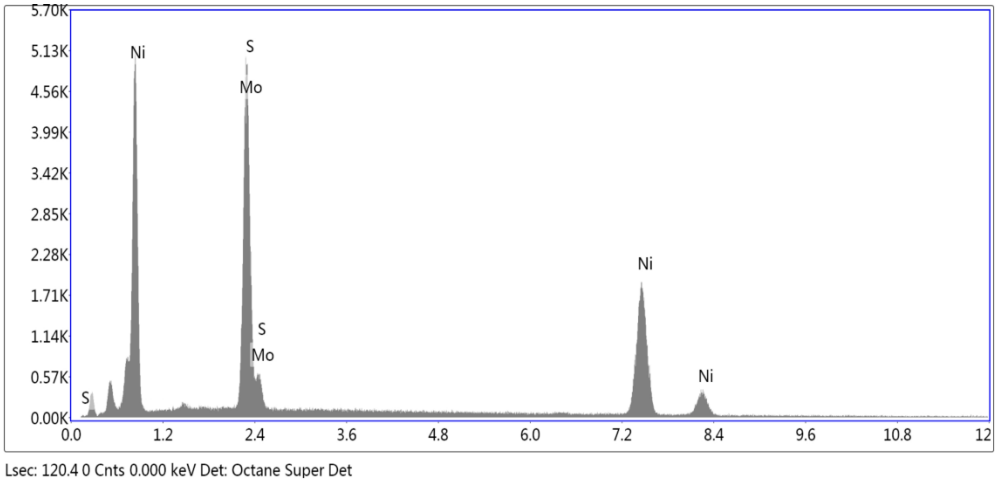

Fig. S5 EDX spectra of Ni-Mo-S.

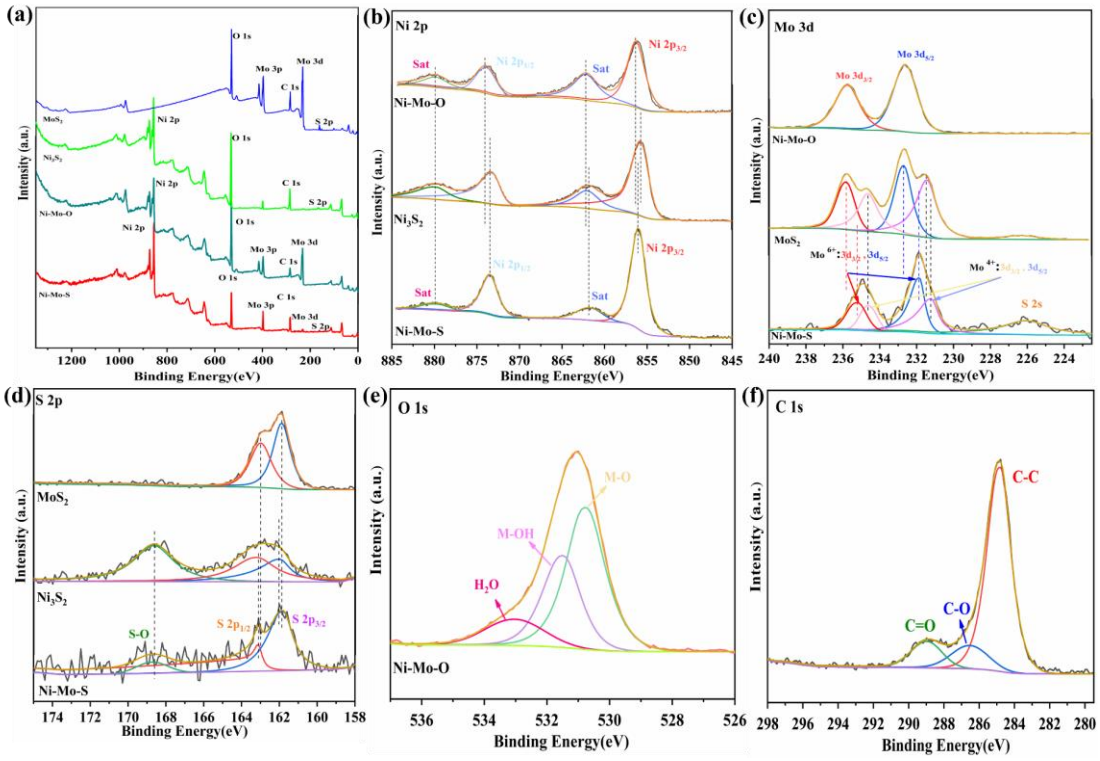

Fig. S6 (a) XPS survey spectrum of Ni-Mo-S, Ni-Mo-O, Ni_3S_2/NF and MoS_2/CC. (b) The high-resolution XPS spectra of Ni 2p for Ni-Mo-S, Ni-Mo-O and Ni_3S_2/NF. (c) Mo 3d for Ni-Mo-S, Ni-Mo-O and MoS_2/CC, (d) S 2p for Ni-Mo-S, Ni_3S_2/NF and MoS_2/CC, (e) O1s for Ni-Mo-O, and (f) C1s for Ni-Mo-S.

Fig. S7 (a) Contact Angle of HMF on Ni foam, (b) Ni-Mo-O and (c) Ni-Mo-S electrode surface.

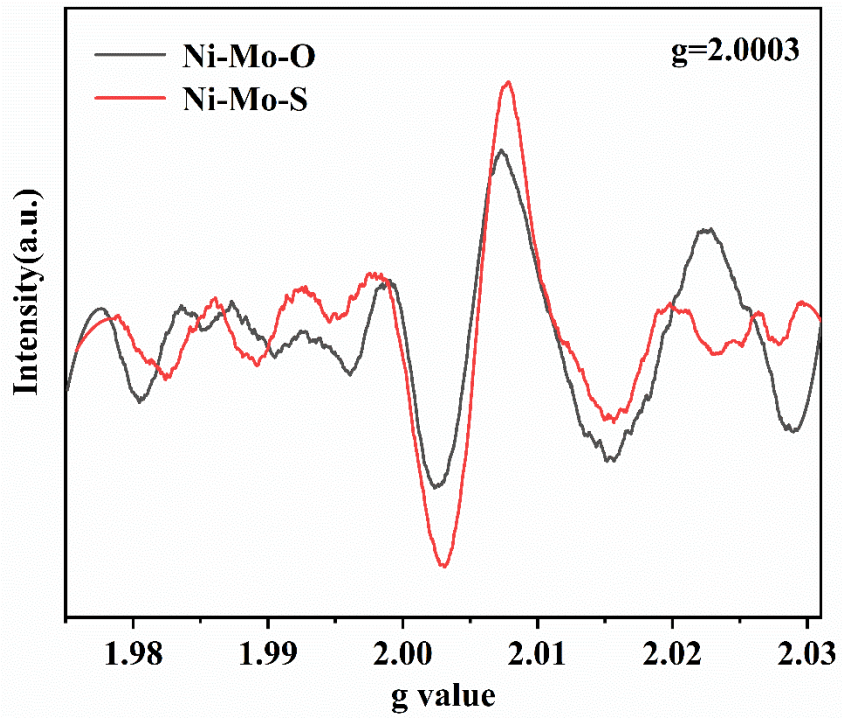

Fig. S8 EPR spectra of Ni-Mo-O and Ni-Mo-S.

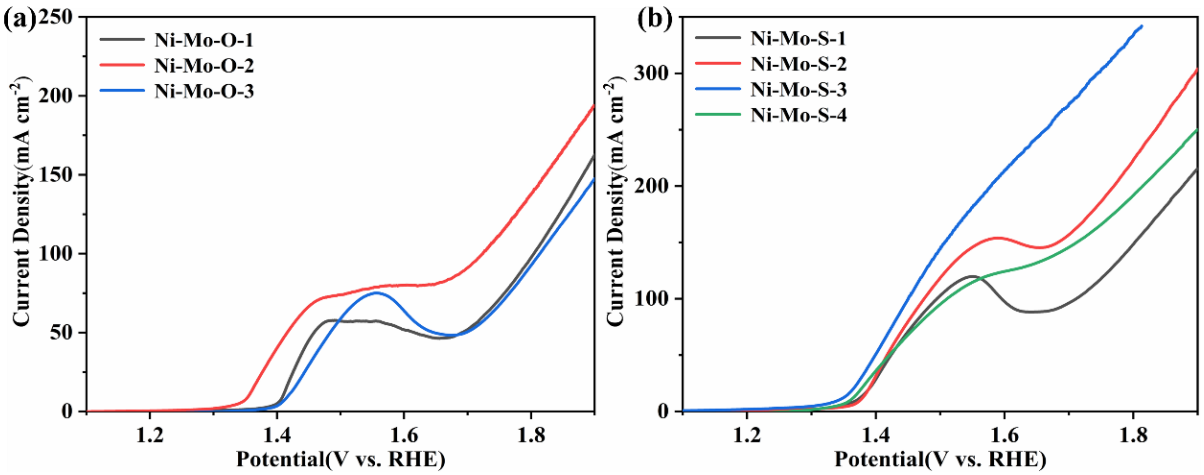

Fig. S9 LSV curves in the presence of 20 mM HMF of (a)Ni-Mo-O-1, Ni-Mo-O-2 and Ni-Mo-O-3, (b) Ni-Mo-S-1, Ni-Mo-S-2, Ni-Mo-S-3 and Ni-Mo-S-4.

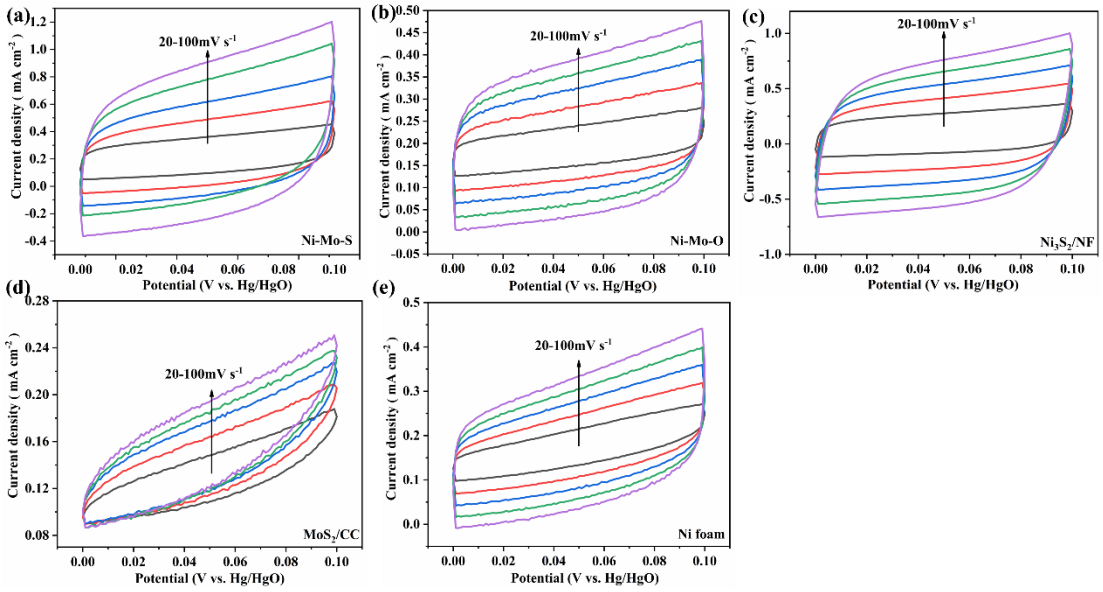

Fig. S10 The Cyclic voltammograms within the range of no faradaic reactions of tri-layered at different scanning rates for (a) Ni-Mo-S, (b) Ni-Mo-O, (c) Ni_3S_2/NF, (d) MoS_2/CC and (e) Ni foam.

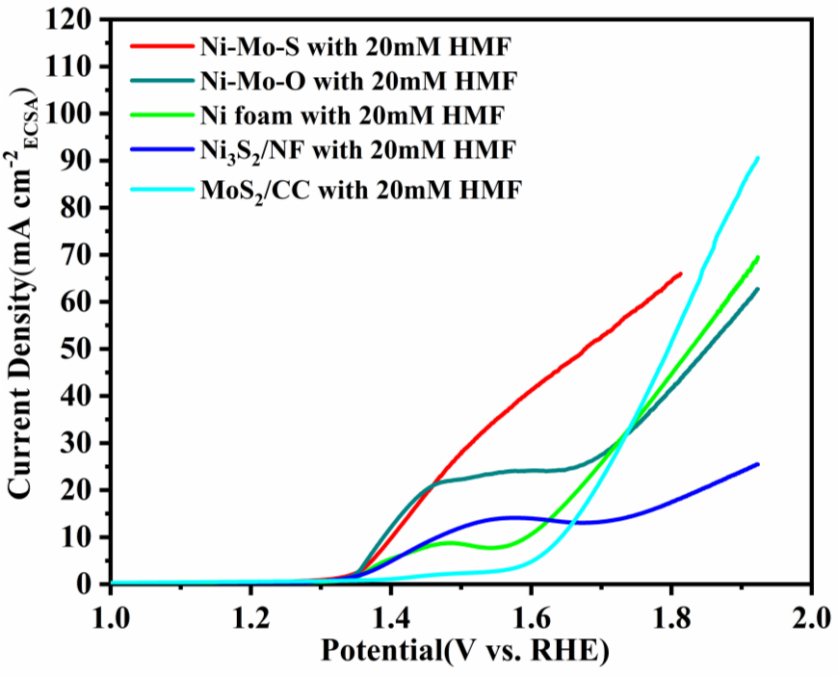

Fig. S11 Normalized LSV curve from Figure. 5b to ECSA with 20mM HMF.

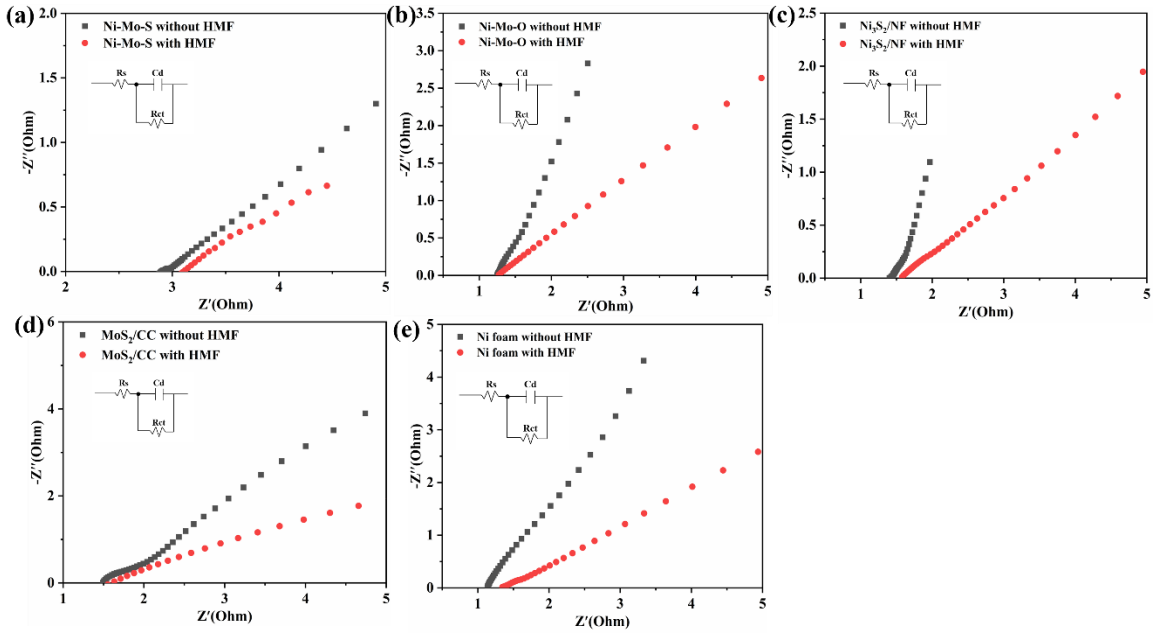

Fig. S12 The Nyquist plots over the (a) Ni-Mo-S, (b) Ni-Mo-O, (c) Ni_3S_2/NF, (d) MoS_2/CC and (e) Ni foam electrocatalysts in 1.0 M NaOH with and without 20mM HMF.

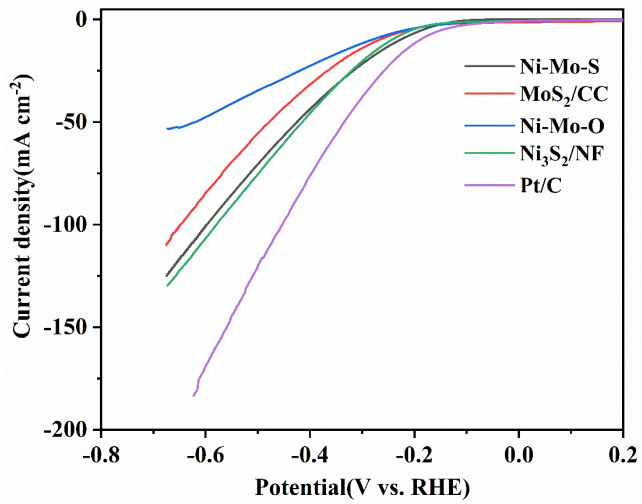

Fig. S13 LSV curves for Ni-Mo-S, Ni-Mo-O, MoS_2/CC, Ni_3S_2/NF and commercial Pt/C cathode HER in 1.0 M NaOH solution.

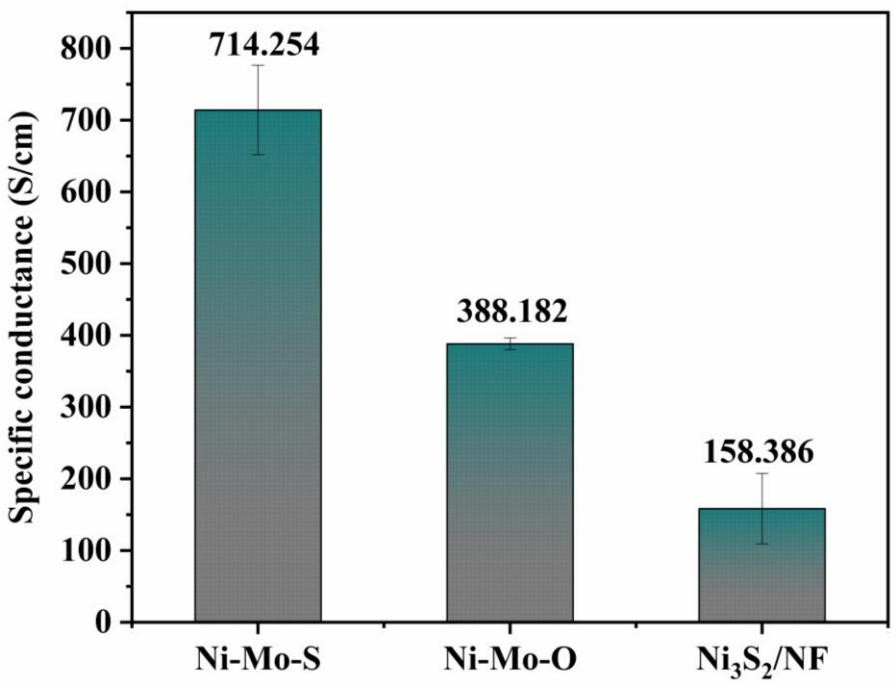

Fig. S14 Results recorded by four-probe resistance for Ni-Mo-S, Ni-Mo-O, and Ni_3S_2/NF[a].

[a]The resistance test adopts the standard four-probe method, using ST2258C multifunctional digital four-probe tester. Each sample tested data at five evenly distributed sites.

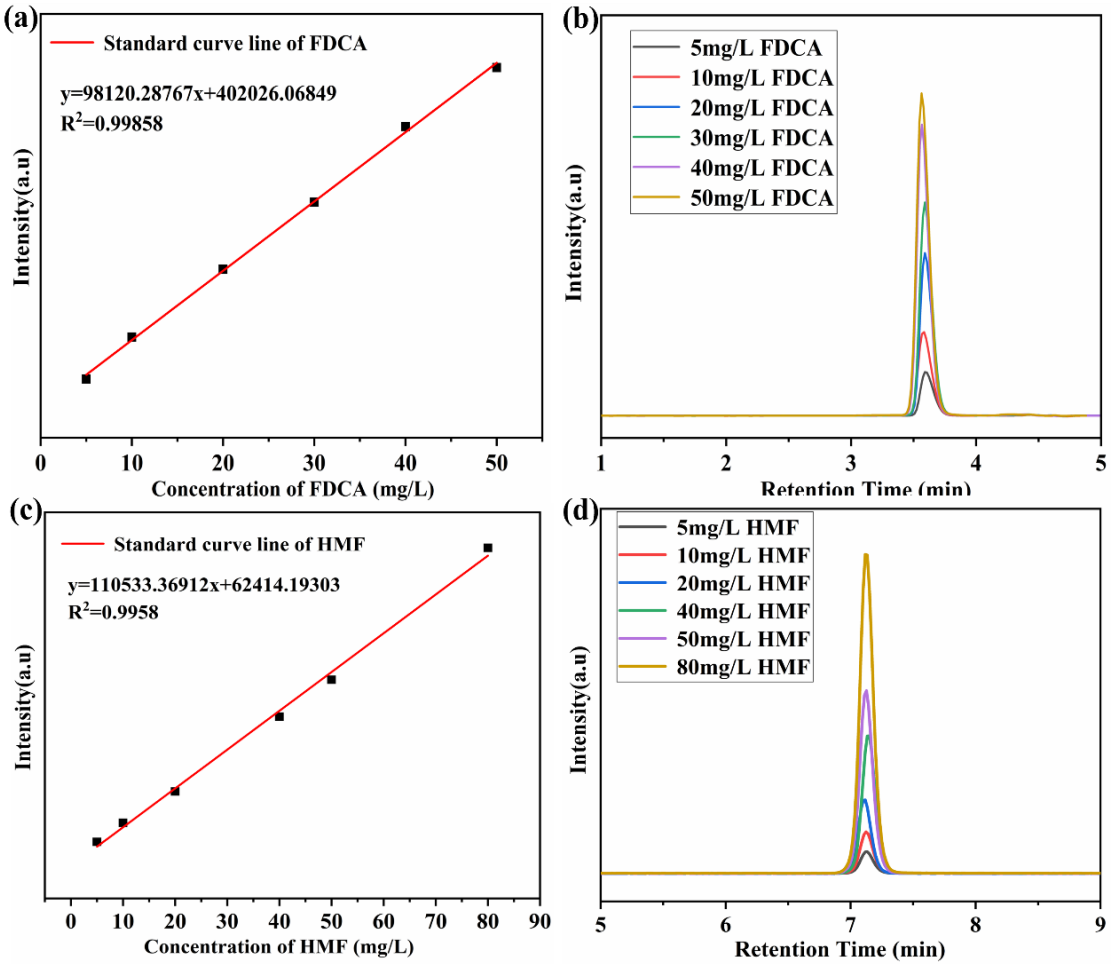

Fig. S15 HPLC chromatogram of standard samples at different concentrations: (a) FDCA, (c) HMF. Calibration of the HPLC for (b) FDCA, (d) HMF.

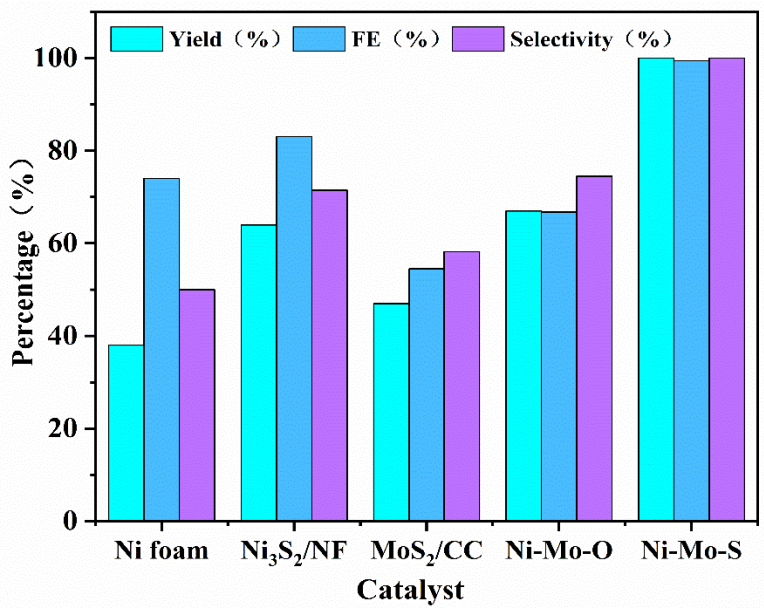

Fig. S16 HMF oxidation yield, Faraday efficiency, and selectivityof the Ni foam, Ni_3S_2/NF, MoS_2/CC, Ni-Mo-O precursor, and $Ni_9S_8/MoS_2/Ni_3S_2$.

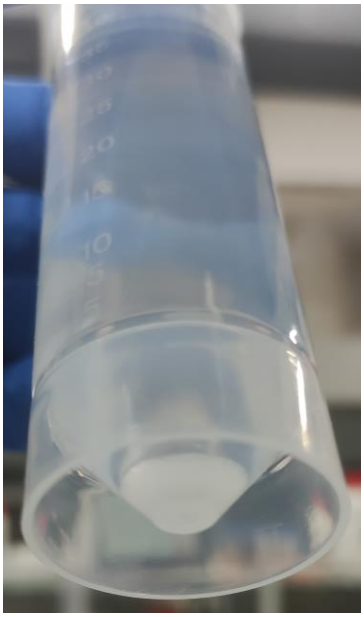

Fig. S17 Diagram of solid products precipitated by sufficient acidification after electrooxidation of HMF.

^{1}H NMR (400 MHz, DMSO-d_6) δ 7.30 (s, 2H).

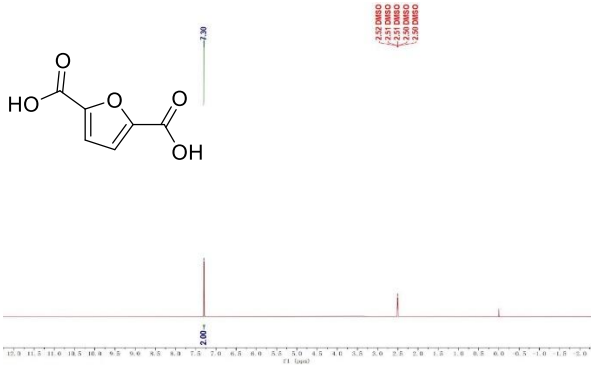

Fig. S18 ^{1}H-NMR spectra of the precipitated solid products in Fig. S9.

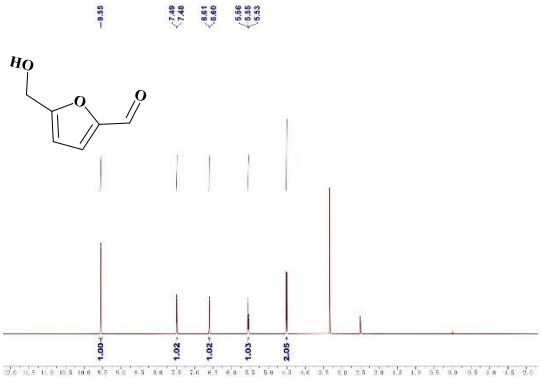

Fig. S19 ^{1}H-NMR spectra of HMF raw material.

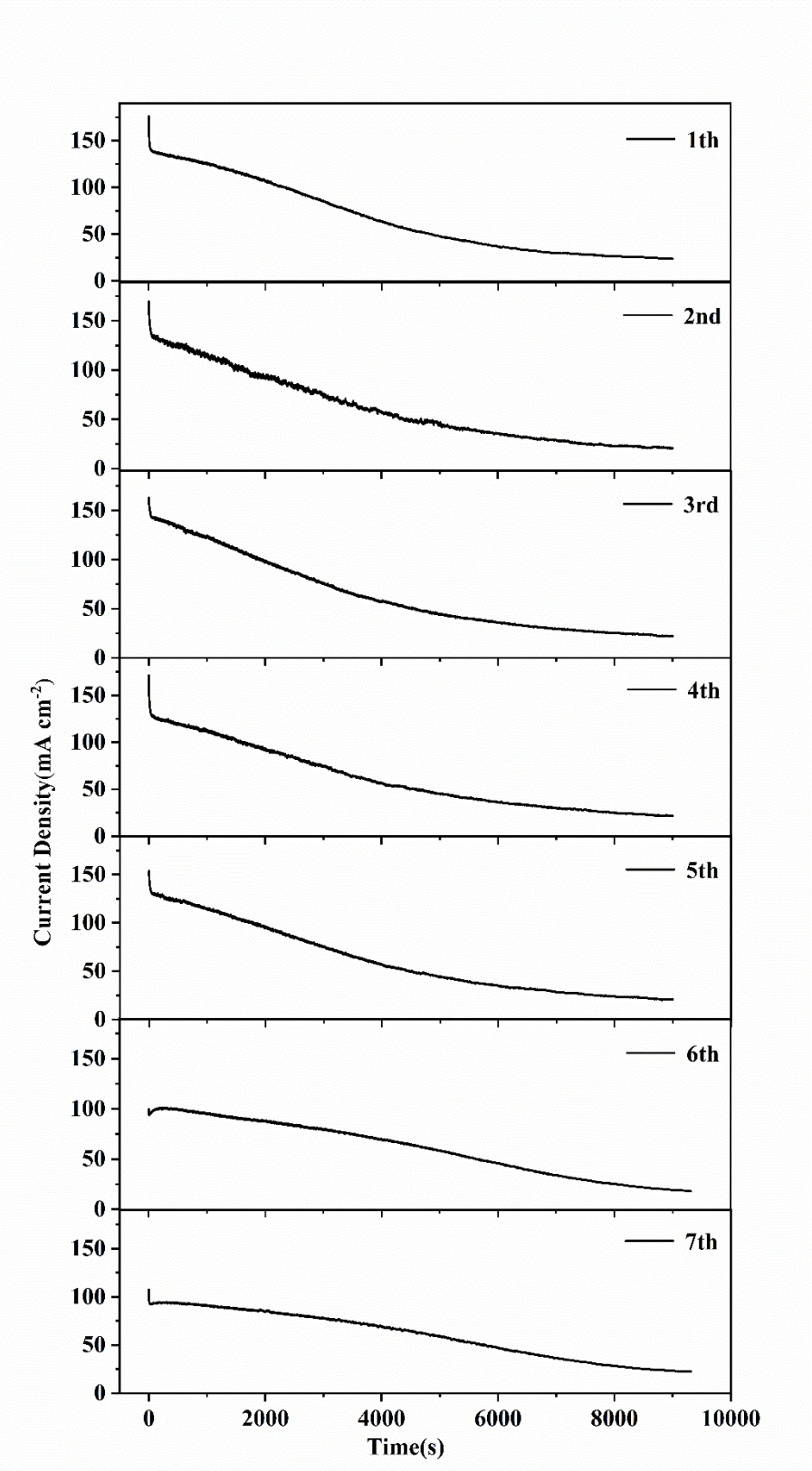

Fig. S20 The i-t curves of HMF oxidation for Ni-Mo-S at a constant potential of 1.52 V (vs. RHE) for the seven successive cycles.

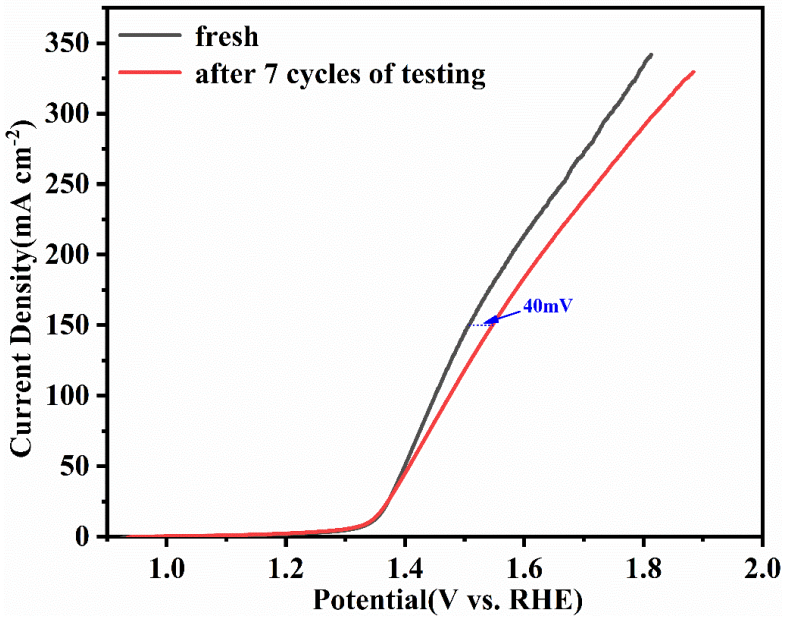

Fig. S21 The LSV curves of Ni-Mo-S with 20mM HMF in1M NaOH

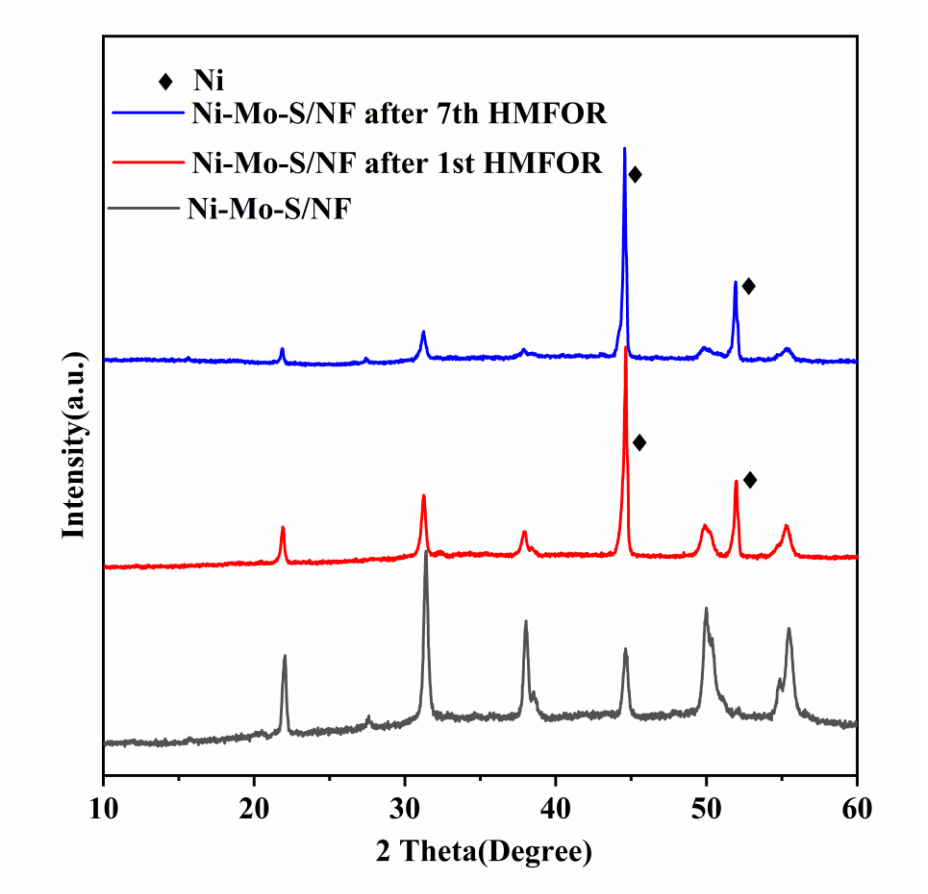

Fig. S22 XRD of the comparison of before and after once/seven times chronoamperometric tests for Ni-Mo-S. (Since the XRD after the reaction is tested on Ni foam, there are more pronounced peaks of Ni (44.5° and 52°))

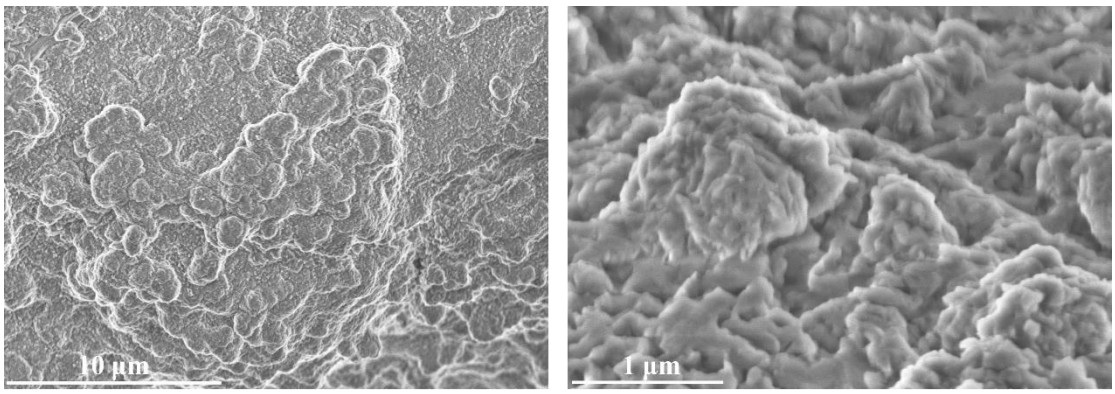

Fig. S23 SEM images of Ni-Mo-S after seven times chronoamperometric tests.

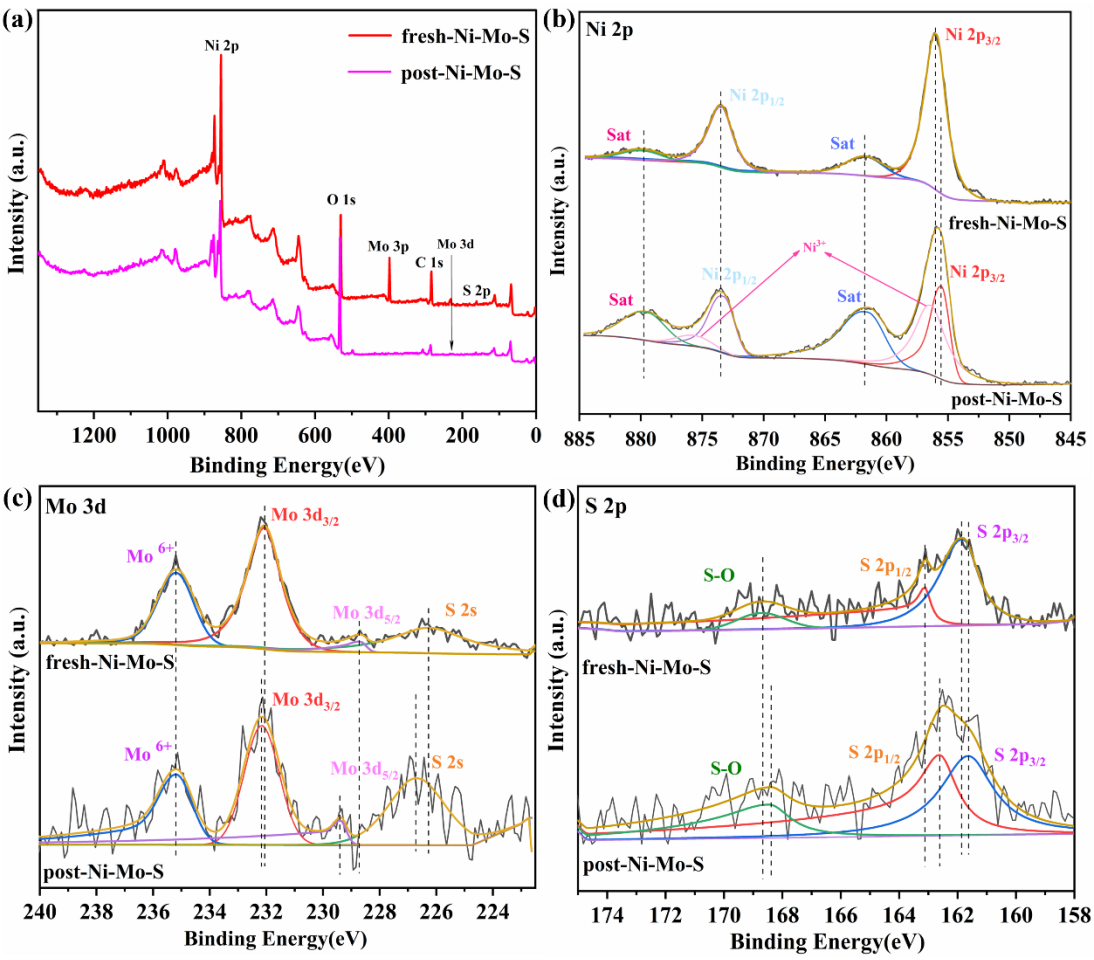

Fig. S24 XPS spectra of Survey full spectra(a), Ni 2p (b), Mo 3d (c) and S 2p (d)

before and after 7 times HMF oxidation.

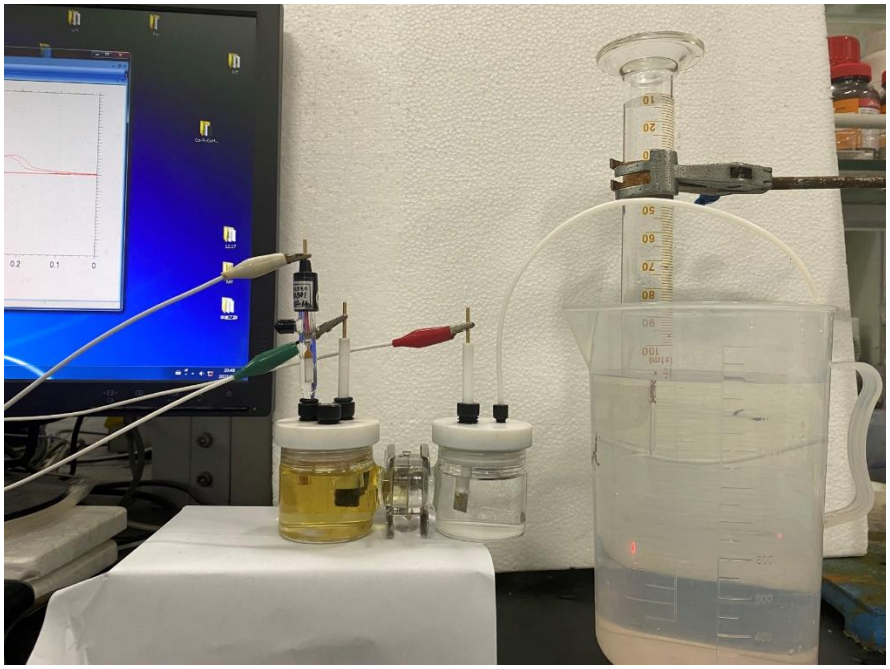

Fig. S25 Diagram of hydrogen collection device in the cathode.

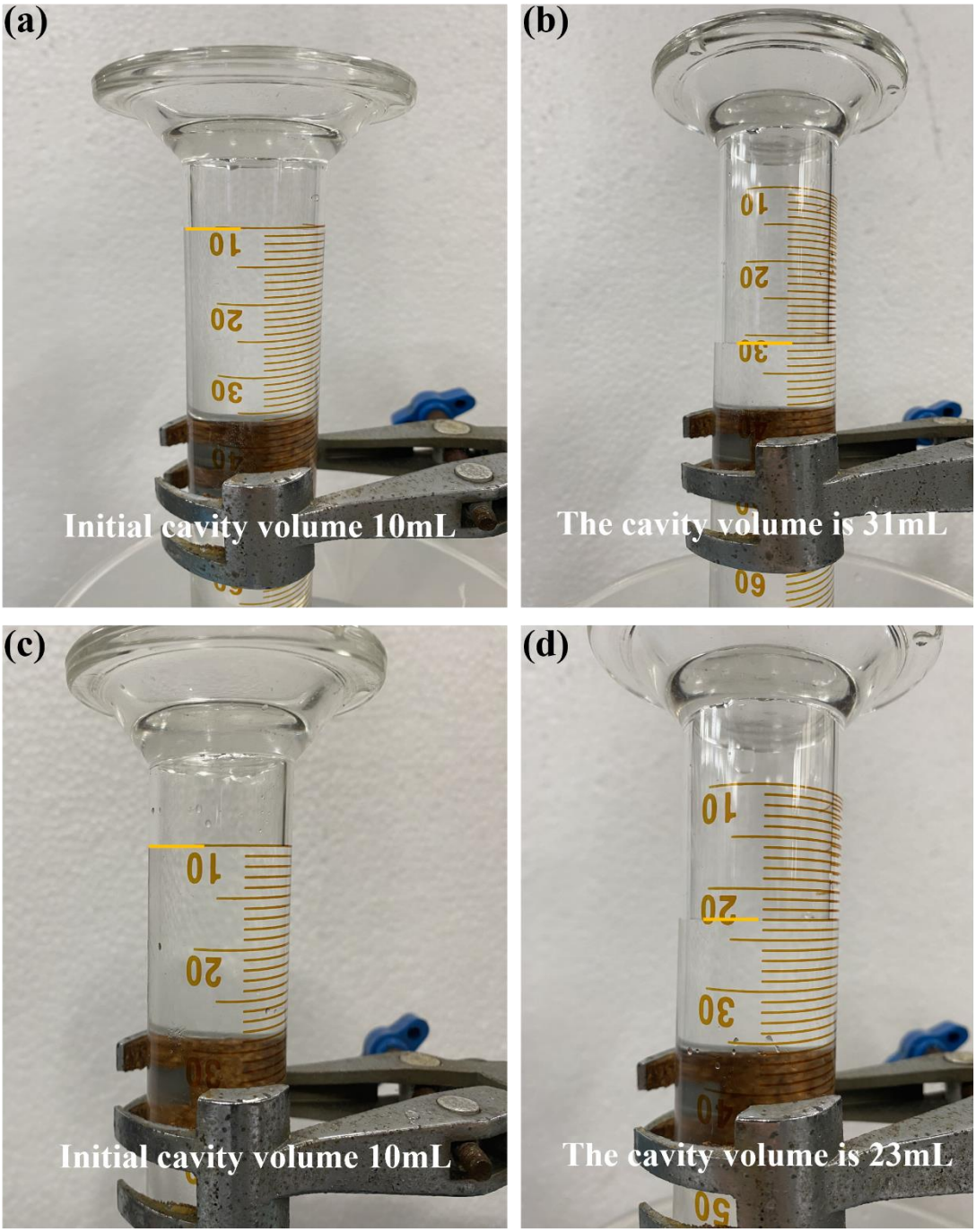

Fig. S26 Hydrogen is collected by drainage (a-b) at 1.52 V (vs. RHE), Ni-Mo-S collects hydrogen at the cathode in the OER process for one hour. (c-d) at 1.52 V (vs. RHE), Ni-Mo-S collects hydrogen at the cathode in the HMFOR process for 10 minures with 1.0 M NaOH+20mM HMF.

Table S1. ICP-OES test of Ni-Mo-S catalyst.

element	Sample element content （mg/kg)	Sample element content （%)
Mo	149091.12	14.91%
Ni	548334.84	54.83%
S	302574.04	30.257%

Table S2. FWHM, area ratio and atomic ratio of each element in Ni-Mo-S, Ni-Mo-O, MoS_2/CC and Ni_3S_2/NF.

	FWHM/eV	Area/CPS.eV	Atomic/%
Ni-Mo-S			
Ni 2p	2.14	122099.5	63.56
Mo 3d	0.99	1295.23	6.20
S 2p	2.24	2016.96	16.70
C 1s	2.48	981.93	5.14
O 1s	2.09	74877.3	8.40
Ni-Mo-O			
Ni 2p	2.48	79502.76	23.16
Mo 3d	1.5	33776.35	14.93
O 1s	1.47	45453.2	51.37
C 1s	1.6	5340.98	10.54
MoS_2/CC			
Mo 3d	1.11	72474.12	13.15
S 2p	1.09	8765.08	11.3
C 1s	1.51	35642.6	36.12
O 1s	2.84	819807.48	40.80

Ni_3S_2/NF			
Ni 2p	2.47	123926.93	31.89
S 2p	2.02	10018.73	18.88
C 1s	3.06	165761.89	22.81
O 1s	3.03	467222.61	26.42

Table S3. Impedance fitting results of as-prepared Ni-Mo-S, Ni-Mo-O, Ni_3S_2/NF, MoS_2/CC and IrO_2/CC.

	R_s/Ω cm^{-2}	R_{ct}/Ω cm^{-2}
Ni-Mo-S	0.99	1.06
Ni-Mo-O	1.27	1.11
Ni_3S_2/NF	2.17	1.56
MoS_2/CC	2.85	6.73
Ni foam	2.59	10.87
IrO_2/CC	2.71	8.87

Table S4. Comparison of Ni-Mo-S with other electrocatalysts for HMFOR.

Catalysts	HMF (mM)	Conversion (%)	FDCA yield (%)	FE (%)	Potenial (V vs. RHE)	Ref.
Pd_1Au_2/C	20	100	83	NA	0.90	[1]

$(AuPd)_7$	5	49.3	11.1	72.8	0.82	[2]
AuNi	10	100	90	99	0.40(vs Ag/AgCl)	[3]
Ir-Co_3O_4	10	100	98	98	1.42	[4]
Co_3O_4	10	100	94.9	94.6	1.40	[5]
Ni_2P NPA/NF	10	100	98	98	1.423	[6]
CoO-$CoSe_2$	10	100	99	97.9	1.43	[7]
NiSe@NiO_x	10	98	97	96	1.423	[8]
NiOOH/FTO	5	99.8	96	96	1.47	[9]
Ni_3S_2/NF	10	100	98	98	1.423	[10]
$NiCo_2O4$	5	99.6	90.4	87.5	1.50	[11]
Ni/NiOOH	650	100	89	80	1.55	[12]
CoB/NF	10	100	94	98	1.45	[13]
$CuNi(OH)_2$/C	5	98.8	93.3	94.4	1.45	[14]
MoO_2-FeP@C	10	99.4	98.6	97.8	1.424	[15]
Cu_xS@NiCo-LDH	10	100	99	99	1.32	[16]
N-$NiMoO_4$	10	100	97	97	1.473	[17]
Ni_3S_2-MoS_2/NF	20	100	99	99	1.45	[18]
Ni-Mo-S	20	100	99.8	99.5	1.52	This work

References

[1] D. J. Chadderdon, L. Xin, J. Qi, Y. Qiu, P. Krishna, K.L. More, W. Li, Green Chem. 2014, **16**, 3778-3786.

[2] M. Park, M. Gu, B. S. Kim, ACS Nano, 2020, **14**, 6812-6822.

[3] N. Heidary, N. Kornienko, Chem. Sci. 2020, **11**, 1798-1806.

[4] Y. Lu, T. Liu, C.L. Dong, Y.C. Huang, Y. Li, J. Chen, Y. Zou, S. Wang, Adv. Mater. 2021, **33**, e2007056.

[5] C. Chen, Z. Zhou, J. Liu, B. Zhu, H. Hu, Y. Yang, G. Chen, M. Gao, J. Zhang, Appl. Catal. B Environ. 2022, **307**, 121209.

[6] B. You, N. Jiang, X. Liu, Y. Sun, Angew. Chem. Int. Ed. Engl. 2016, **55**, 9913-9917.

[7] X. Huang, J. Song, M. Hua, Z. Xie, S. Liu, T. Wu, G. Yang, B. Han, Green Chem. 2020, **22**, 843-849.

[8] L. Gao, Z. Liu, J. Ma, L. Zhong, Z. Song, J. Xu, S. Gan, D. Han, L. Niu, Appl. Catal. B Environ. 2020, **261**, 118235.

[9] B. J. Taitt, D.-H. Nam, K.-S. Choi, ACS Catal. 2018, **9**, 660-670.

[10] B. You, X. Liu, N. Jiang, Y. Sun, J. Am. Chem. Soc. 2016, **138**, 13639-13646.

[11] M. J. Kang, H. Park, J. Jegal, S.Y. Hwang, Y.S. Kang, H.G. Cha, Appl. Catal. B Environ. 2019, **242**, 85-91.

[12] R. Latsuzbaia, R. Bisselink, A. Anastasopol, H. van der Meer, R. van Heck, M.S. Yagüe, M. Zijlstra, M. Roelands, M. Crockatt, E. Goetheer, E. Giling, J. Appl. Electrochem. 2018, **48**, 611-626.

[13] J. Weidner, S. Barwe, K. Sliozberg, S. Piontek, J. Masa, U.P. Apfel, W. Schuhmann, Beilstein. J. Org. Chem. 2018, **14**, 1436-1445.

[14] H. Chen, J. T. Wang, Y. Yao, Z. H. Zhang, Z. Z. Yang, J. Li, K.Q. Chen, X. Y. Lu, P.K. Ouyang, J. Fu, Chemelectrochem, 2019, **6**, 5797-5801.

[15] G. C. Yang, Y. Q. Jiao, H. J. Yan, Y. Xie, A. P. Wu, X. Dong, D. Z. Guo, C. G. Tian, H. G. Fu, Adv. Mater. 2020, **32**, 2000455.

[16] X. Deng, X. Kang, M. Li, K. Xiang, C. Wang, Z. Guo, J. Zhang, X.-Z. Fu, J.-L. Luo, J. Mater. Chem. A, 2020, **8**,1138-1146.

[17] W. Wang, M. Wang, Catal. Sci. Technol. 2021, **11**, 7326-7330.

[18] S. Yang, Y. Guo, Y. Zhao, L. Zhang, H. Shen, J. Wang, J. Li, C. Wu, W. Wang, Y. Cao, S. Zhuo, Q. Zhang, H. Zhang, Small, 2022, **18**, e2201306.